IOP PUBLISHING METROLOGIA
Metrologia **46** (2009) 87–94 doi:10.1088/0026-1394/46/1/011

Operating an atom interferometer beyond its linear range

S Merlet[1], J Le Gouët[1], Q Bodart[1], A Clairon[1], A Landragin[1], F Pereira Dos Santos[1] and P Rouchon[2]

[1] LNE-SYRTE, CNRS UMR 8630, UPMC, Observatoire de Paris, 61 avenue de l'Observatoire, 75014 Paris, France
[2] Mines ParisTech, Centre Automatique et Systèmes, 60, bd Saint-Michel, 75272 Paris Cedex 06, France

E-mail: franck.pereira@obspm.fr

Received 30 May 2008, in final form 22 October 2008
Published 6 January 2009
Online at stacks.iop.org/Met/46/87

Abstract
In this paper, we show that an atom interferometer inertial sensor, when associated with the auxiliary measurement of external vibrations, can be operated beyond its linear range and still keep a high acceleration sensitivity. We propose and compare two measurement procedures (fringe fitting and non-linear lock) that can be used to extract, without adding any bias, the mean phase of the interferometer when the interferometer phase fluctuations exceed 2π. Despite operating in the urban environment of inner Paris without any vibration isolation, the use of a low noise seismometer for the measurement of ground vibrations allows our atom gravimeter to reach at night a sensitivity as good as $5.5 \times 10^{-8} g$ at 1 s. Robustness of the measurement to large vibration noise is also demonstrated by the ability of our gravimeter to operate during an earthquake with excellent sensitivity. For such low vibration frequency though, high pass filtering of the seismometer degrades its correlation with the interferometer signal, so that low frequency seismic vibrations appear on the gravity measurement. Nevertheless, our high repetition rate allows for efficient sampling of these perturbations, ensuring proper averaging. Such techniques open new perspectives for applications in other fields, such as navigation and geophysics.

(Some figures in this article are in colour only in the electronic version)

1. Introduction

Atom interferometers [1] are used to develop highly sensitive inertial sensors, which compete with state of the art 'classical' instruments [2]. Applications of such interferometers cover numerous fields, from fundamental physics [3–7] to navigation and geophysics. For instance, transportable devices are being developed with foreseen applications in the fields of navigation, gravity field mapping, detection of underground structures etc.

In most of these experiments, atomic waves are separated and recombined using two-photon transitions, induced by a pair of counterpropagating lasers. The inertial force is then derived from the measurement of the relative displacement of free-falling atoms with respect to the lasers' equiphase, which provide a precise ruler. As the inertial phase shift scales quadratically with the interrogation time, very high sensitivities can be reached using cold atoms along parabolic trajectories [8, 9], provided that the experiments are carefully shielded from ground vibrations. In the usual geometry where the laser beams are retroreflected on a mirror, the position of this mirror sets the position of the lasers' equiphase, so that only this 'reference' optical element is to be shielded from ground vibrations. Such an isolation can be realized either with an active stabilization scheme, using a long period superspring [2, 10, 11], or by using a passive isolation platform [12]. For instance, the use of a superspring allowed the interaction time to be increased to 800 ms and permitted a best short term sensitivity to acceleration of $8 \times 10^{-8}\,\mathrm{m\,s^{-2}}$ at 1 s [13]. An alternative technique, which we study in this paper, does not require any vibration isolation, but exploits an independent measurement of ground vibrations, realized by a low noise accelerometer, in order to correct for their impact on the gravity measurement. This technique is based on a simple idea: any measurement corrupted by parasitic vibrations can in principle be efficiently corrected from them, providing these vibrations

are measured and the transfer function of vibrations on the quantity of interest is known. It could thus be applied to light interferometers or to lasers stabilized on high finesse cavities, for instance. A technique based on the same principle has already been used with a 'classical' corner cube gravimeter [14, 15] and allowed its sensitivity to be improved by a factor of 7 [15].

In this paper, we investigate the limits to the sensitivity of an atomic gravimeter when operating without vibration isolation. This transportable gravimeter is developed within the frame of the watt balance project led by the Laboratoire National de Métrologie et d'Essais (LNE) [16, 17]. We first briefly describe our experimental setup and recall the usual procedures for measuring the mean phase of the interferometer. We then introduce and compare two measurement schemes (fringe fitting and non-linear lock) that allow the sensor to be operated in the presence of large vibration noise and show how phase measurements can be performed even though the interferometer phase noise amplitude exceeds 2π. These schemes, which use an independent measurement of vibration noise with a low noise seismometer, allow good sensitivities to be achieved without vibration isolation. In particular, we reach a sensitivity as good as $5.5 \times 10^{-8} g$ at 1 s during night measurements, in the urban environment of inner Paris. Finally, the robustness of these measurement schemes versus changes in the vibration noise is illustrated by the capability of our instrument to operate and measure large ground accelerations induced by an earthquake.

2. Limits due to vibration noise in a conventional setup

2.1. Experimental setup

The experimental setup, which we briefly recall here, has been described in detail in [12, 18]. About 10^7 ^{87}Rb atoms are first loaded in a 3D-MOT (magneto-optical trap) within 50 ms, and further cooled down to 2.5 μK before being dropped in free fall. Before creating the interferometer, a narrow vertical velocity distribution of width about 1 cm s^{-1} is selected in the $|F = 1, m_F = 0\rangle$ state, using several microwave and optical Raman pulses.

The interferometer is then created using Raman transitions [8] between the two hyperfine levels $F = 1$ and $F = 2$ of the $^5S_{1/2}$ ground state, which are induced by two vertical and counterpropagating laser beams of frequencies ω_1, ω_2 and wavevectors $\vec{k}_1, \vec{k}_2$. A sequence of three Raman pulses ($\pi/2 - \pi - \pi/2$) allows one to split, redirect and recombine the atomic wave packets. The relationship between external and internal state [1] allows one to measure the interferometer phase shift from a fluorescence measurement of the populations of each of the two states. At the output of the interferometer, the transition probability P from one hyperfine state to the other is given by $P = a + b \cos \Delta\Phi$, where $2b$ is the interferometer contrast, and $\Delta\Phi$, the difference in the atomic phases accumulated along the two paths, is given by $\Delta\Phi = -\vec{k}_{\text{eff}} \cdot \vec{g} T^2$ [19]. Here $\vec{k}_{\text{eff}} = \vec{k}_1 - \vec{k}_2$ is the effective wave vector (with $|\vec{k}_{\text{eff}}| = k_1 + k_2$ for counterpropagating beams), T is the time interval between two consecutive pulses and g is the acceleration of gravity.

The Raman light sources are two extended cavity diode lasers based on the design of [20], which are amplified by two independent tapered amplifiers. Their frequency difference, which is phase locked onto a low phase noise microwave reference source, is swept according to $(\omega_2 - \omega_1)(t) = (\omega_2 - \omega_1)(0) + \alpha t$ in order to compensate for the gravity-induced Doppler shift. This adds αT^2 to the interferometer phase shift, which eventually cancels it for a perfect Doppler compensation, for which $\alpha_0 = \vec{k}_{\text{eff}} \cdot \vec{g}$.

2.2. Conventional measurement procedures

Maximal sensitivity to phase fluctuations is achieved when operating the interferometer at mid-fringe, which corresponds to $\Delta\Phi = \pm\pi/2$. In this case, though, variations in the offset a can be interpreted as fluctuations of the interferometer phase. A standard technique [10] then consists in recording a full fringe, by measuring the transition probability as a function of a controlled phase shift induced on the interferometer. Fitting this fringe then allows g to be measured. This technique degrades the short term sensitivity as measurements performed at the top or bottom of the fringes are not sensitive to phase fluctuations. An alternative way consists of using a method inspired by microwave atomic clocks. The phase is modulated by $\pm\pi/2$ so that the measurement is always performed at mid-fringe, alternatively to the right and to the left side of the central fringe. From two consecutive measurements P_i and P_{i+1}, the phase error can be estimated. In practice, a correction $G \times (P_i - P_{i+1})$ is added at each cycle to α, in order to steer the chirp rate onto the central fringe. This realizes an integrator, whose time constant can be set to a few cycles by adjusting the gain G. This locking technique has the advantage of rejecting offset and contrast fluctuations, while preserving maximal sensitivity to phase fluctuations.

2.3. Influence of vibration noise

In the case where the duration of the Raman pulses can be neglected, the phase shift $\Delta\Phi$ induced by vibrations is given by

$$\begin{aligned}\Delta\Phi &= k_{\text{eff}}(z_g(-T) - 2z_g(0) + z_g(T)) \\ &= k_{\text{eff}} \int_T^{-T} g_s(t) v_g(t)\, \mathrm{d}t, \end{aligned} \tag{1}$$

where z_g and v_g are the position and velocity of the experimental setup, and g_s is the sensitivity function [21], given by

$$g_s(t) = \begin{cases} -1 & -T < t < 0, \\ 1 & 0 < t < T. \end{cases} \tag{2}$$

The expected sensitivity of the interferometer to g fluctuations of the interferometer is then given by a weighted sum of the vibration noise at the harmonics of the cycling rate f_c [21]:

$$\sigma_g^2(\tau) = \frac{1}{\tau} \sum_{k=1}^{\infty} \left(\frac{\sin(\pi k f_c T)}{\pi k f_c T} \right)^4 S_a(2\pi k f_c), \tag{3}$$

where $\sigma_g(\tau)$ is the Allan standard deviation of acceleration fluctuations for an averaging time τ and S_a is the power spectral density of acceleration fluctuations.

Figure 1 displays the power spectral densities of vibrations, measured with a low noise seismometer (Guralp CMG-40T, response option 30 s) on the platform which is either floating (ON) (day time) or put down (OFF) (day time and night time). In the case where the platform is OFF, the spectrum is similar to the spectrum measured directly on the ground. For our typical parameters, $2T = 100$ ms and $f_c = 3.8$ Hz, we calculate using equation (3) sensitivities at $\tau = 1$ s of $2.9 \times 10^{-6} g$ during the day and $1.4 \times 10^{-6} g$ during the night with the platform OFF. With the platform ON, the sensitivity is expected to be $7.6 \times 10^{-8} g$.

3. Vibration noise correction

3.1. Correlation between atomic and seismometer signals

The signal of the seismometer can be used to determine the phase shift of the interferometer due to residual vibrations, as measured by the seismometer, $\phi^S_{\rm vib}$, which is given by

$$\phi^S_{\rm vib} = k_{\rm eff} \int_T^{-T} g_{\rm s}(t) v_{\rm s}(t)\, {\rm d}t = k_{\rm eff} K_{\rm s} \int_T^{-T} g_{\rm s}(t) U_{\rm s}(t)\, {\rm d}t, \tag{4}$$

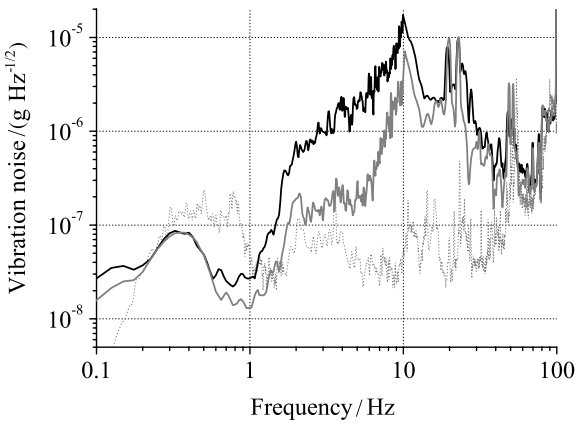

Figure 1. Amplitude spectral densities of vibration noise. The black (respectively, grey) thick curve displays the vibration noise with the isolation platform down (OFF) at day time (respectively night time), while the dotted curve displays the vibration noise with the floating platform (ON) at day time.

where $U_{\rm s}$ is the seismometer voltage (velocity) output and $K_{\rm s} = 400.2\ {\rm V\,m^{-1}\,s^{-1}}$ is the velocity output sensitivity of the seismometer.

Figure 2 displays the measured transition probability as a function of $\phi^S_{\rm vib}$, in the two cases of platform ON and OFF, for an interferometer time $2T = 100$ ms. The noise is low enough in the ON case (figure 2(*b*)) for the interferometer to operate close to mid-fringe, while in the OFF case (figure 2(*a*)) interferometer phase noise is larger than 2π, and the interferometer signal jumps from one fringe to another. Figure 2 shows the good correlation between measured and calculated phase shifts. In the ON case, we find a correlation factor as high as 0.94.

The calculated $\phi^S_{\rm vib}$ can thus be used to significantly improve the sensitivity of the measurement, by applying a post-correction on the transition probability measured at mid-fringe. This correlation is not perfect though due to the response function of the seismometer, which is not flat, and behaves like a low-pass filter with a cut-off frequency of 50 Hz. This response function thus limits the efficiency of the vibration rejection. Figure 3 displays as a continuous black line the rejection efficiency as a function of frequency, which is calculated from the seismometer transfer function.

3.2. Digital filtering

We implemented a numerical filtering of the seismometer signal to compensate for the phase lag of the seismometer at intermediate frequencies. The design of the filter is described in detail in [12]. It consists of the product of a recursive infinite impulse response (IIR) filter, with corner frequencies f_0 and f_1, and a non-causal low-pass filter. The IIR filter compensates the phase shift of the seismometer signal and the non-causal filter prevents the IIR filter from amplifying the intrinsic noise of the seismometer at high frequencies, without affecting the phase advance needed to improve the rejection. The total transfer function of the filter is given by

$$F(f) = \frac{1 + jf/f_0}{1 + jf/f_1} \frac{1}{1 + (f/f_{\rm c})^2}, \tag{5}$$

where f_0, f_1 and $f_{\rm c}$ are then optimized in order to reach the best sensitivity. This digital filtering significantly improves

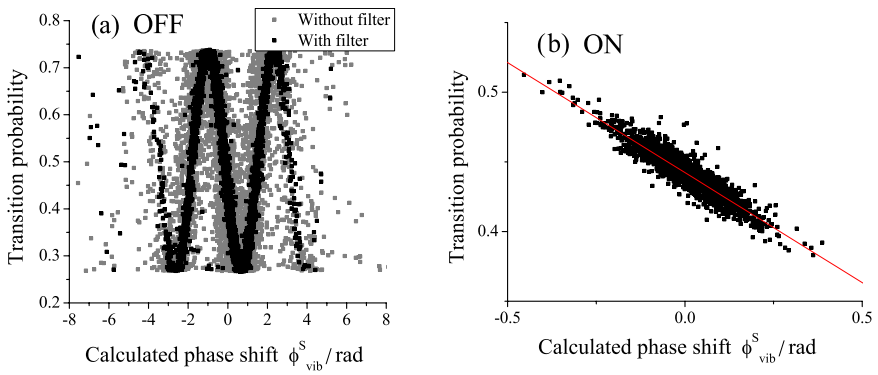

Figure 2. Correlation between the transition probability of the interferometer and the phase shift calculated from the seismometer data, for $2T = 100$ ms. (*a*) The isolation platform is OFF. Grey points: without digital filter, black points: with digital filter. (*b*) The isolation platform is ON. Black points: with digital filter. Line: fit to the data, with correlation factor of 0.94.

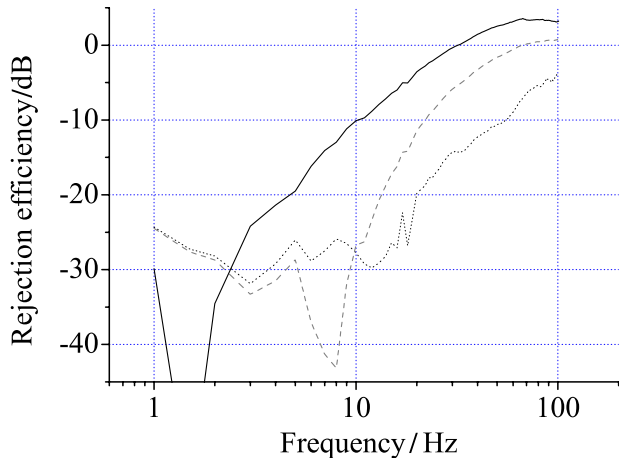

Figure 3. Efficiency of the vibration rejection as a function of frequency without any processing (black straight line), with a digital filter (dashed line), with a compensation of a delay of 4.6 ms (dotted line).

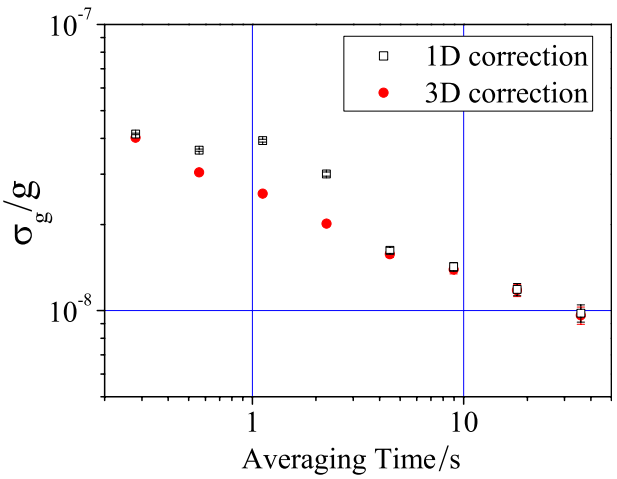

Figure 4. Sensitivity to g with 1D and 3D corrections. The measurement was realized during the day, with a floating platform.

the rejection efficiency, as can be seen in figure 3, where it is displayed as a dashed line, for the frequencies $f_0 = 30$ Hz, $f_1 = 180$ Hz and $f_c = 29$ Hz. Despite this increase in the rejection efficiency, the gain in the sensitivity, when implementing this filter in the ON mode, was limited to 25% only [12], which we attributed to excess noise of the seismometer arising from coupling between the horizontal and the vertical axes.

3.3. Cross couplings

In order to detect these couplings, we recorded simultaneously the seismometer outputs along the three directions, calculated three corrections, one along each axis (only the vertical correction was numerically filtered though) and fitted the transition probability measured at mid-fringe with a linear combination of the three corrections. The result of this fit showed couplings of 4% and 5% with the horizontal axes. We finally determined the influence of these couplings on the sensitivity of the measurement, by comparing the Allan standard deviation of the phase fluctuations in the case where the correction is performed only with the vertical correction (1D) or with the optimal combination of the three (3D). The results are shown in figure 4, where the sensitivity is expressed relative to g.

Using the three corrections allows one to remove a bump that appears when using the 1D correction. This indicates that horizontal vibration noise, as also appears in the vertical seismometer signal, adds noise when performing a 1D correction.

3.4. Efficiency of the filter without vibration isolation

The digital filter is much more efficient in the OFF mode, as one can see in figure 2(*a*) where the noise on the interferometer fringes is significantly reduced when seismometer data are processed with the digital filter. In that case, the dominant contribution of the vibration noise to the degradation of the sensitivity corresponds to frequencies around 10 Hz, for which the effect of the filter improves the rejection efficiency from 10 dB to about 30 dB [12].

3.5. Case of a pure delay

We later noticed that the phase lag of the seismometer signal varies almost linearly with respect to the frequency in the 1 Hz to 100 Hz band, with a slope corresponding to a delay of about 5 ms. The phase shift of the seismometer can thus be compensated for, by simply shifting the acquisition of the seismometer data by this delay. We measured the correlation factor as a function of the delay, with the platform OFF, and found an optimal delay of 4.6 ms. The rejection efficiency for this optimal delay is displayed as a dotted line on figure 3. Surprisingly, we find a correlation similar to the optimal digital filter, despite a significantly different behaviour of the rejection efficiency versus frequency.

4. Measurement protocols

4.1. Standard procedures

The standard measurement protocols described above need phase fluctuations to remain significantly smaller than 2π. This requires the interferometer duration in the OFF mode to be reduced to $2T \leqslant 20$ ms. For $2T = 20$ ms, the integrator scheme described above allows one to reach sensitivities of $1 \times 10^{-5} g$ at 1 s when applying no correction to the measured transition probability, $5 \times 10^{-6} g$ when correcting without filtering and $1.5 \times 10^{-6} g$ when correcting with digital filtering. The simple post-correction (without filter) thus improves the sensitivity by a factor 2, and the digital filter improves it further by a factor 3.5. Better performances are expected with large interrogation time for which the transfer function of the interferometer filters high frequency vibration noise more efficiently. In order to operate the interferometer with large interrogation times despite excess noise, we propose two alternative measurement procedures described in the following subsections. Both are based on the combination of measurements of the transition probability and of $\phi^S_{\rm vib}$ by the

seismometer. Though developed for the case of large vibration noise, these techniques can be extended to low vibration noise by adding a well controlled phase modulation.

4.2. Fringe fitting

The first technique simply consists of fitting fringes, as in [10], except that here the phase of the interferometer is now scanned randomly by vibration noise. The signal displayed in figure 2 and obtained when plotting the transition probability versus $\phi^S_{\rm vib}$, calculated with the digital filter, can be fitted by the function $P = a + b\cos(\eta\phi^S_{\rm vib} + \delta\phi)$, where a, b, η and $\delta\phi$ are free parameters. Due to the influence of the seismometer transfer function, η will in general differ from 1. In practice, we operate the interferometer close to the central fringe, which corresponds to a small phase error $\delta\phi$. Every 20 points, we perform a fit of the signal and extract a value for the phase error $\delta\phi_m$. We then calculate the Allan standard deviation of the $\delta\phi_m$ in order to determine the sensitivity of the measurement. Note that this fitting procedure is not very efficient if the noise amplitude is significantly less than 2π, because the interferometer signal remains close to the bottom of the central fringe. An additional and perfectly controlled phase modulation of $\pm\pi/2$ is thus applied in order to optimize the sensitivity of the interferometer to phase fluctuations. Moreover, the sensitivity improves by about 50% when taking cross couplings of the seismometer into account, which can be realized by adjusting the data with a linear combination of the corrections along three directions $\Sigma\eta_j\phi^S_{{\rm vib},j}$, where $j = x, y, z$ and $\phi^S_{{\rm vib},j}$ is the phase shift calculated from the filtered seismometer data along axis j.

4.3. Non-linear lock

The lock procedure described in section 2.2 can be adapted in the case where the phase noise exceeds 2π. Let us consider the measurement at cycle i of the transition probability P_i

$$\begin{aligned} P_i &= a - b\cos((k_{\rm eff}g - \alpha)T^2 + S_i) \\ &= a - b(\cos e\cos S_i - \sin e\sin S_i), \end{aligned} \tag{6}$$

where $e = (k_{\rm eff}g - \alpha)T^2$ is the phase error and S_i is the phase shift induced by residual vibrations, estimated from the seismometer signal. We assume here that the phase error e varies slowly, so that we can consider it as constant between three consecutive measurements. Eliminating a and $\cos e$ from the following three equations

$$\begin{aligned} P_{i-1} &= a - b(\cos S_{i-1}\cos e - \sin S_{i-1}\sin e), \\ P_i &= a - b(\cos S_i\cos e - \sin S_i\sin e), \\ P_{i+1} &= a - b(\cos S_{i+1}\cos e - \sin S_{i+1}\sin e) \end{aligned}$$

gives

$$bB_i\sin e = A_i$$

with

$$\begin{aligned} A_i &= (\cos S_{i+1} - \cos S_i)(P_{i-1} - P_i) \\ &\quad - (\cos S_{i-1} - \cos S_i)(P_{i+1} - P_i), \\ B_i &= (\cos S_{i+1} - \cos S_i)(\sin S_{i-1} - \sin S_i) \\ &\quad - (\cos S_{i-1} - \cos S_i)(\sin S_{i+1} - \sin S_i). \end{aligned}$$

In order to steer the chirp rate onto the Doppler shift rate, an iterative correction is applied to α according to

$$\alpha_{i+2} = \alpha_{i+1} + K\frac{2B_i}{1 + B_i^2}A_i, \tag{7}$$

where K is a positive gain. Here $\frac{2B_i}{1+B_i^2}$ is used as a pseudo-inverse of bB_i with $b \approx 1/2$, in order to prevent the correction from diverging when B_i is close to zero. Choosing $K < 1/T^2$ guarantees the stability of the servo loop.

4.4. Adaptation of the non-linear lock

When phase fluctuations are significantly less than 1 rad, B_i becomes much smaller than 1 (note that B_i is null in the absence of vibration noise, which implies that the lock scheme does not work, as it is not able to steer the chirp rate), so that $\frac{B_i}{1+B_i^2}$ is not a good pseudo-inverse of B_i. This decreases the effective gain of the loop, which can be compensated for either by increasing K or by replacing $\frac{B_i}{1+B_i^2}$ with $\frac{B_i}{\sigma_B^2+B_i^2}$, where σ_B is the standard deviation of the B_is.

The scheme is then to be modified by adding extra phase shifts in order to increase the sensitivity to phase fluctuations. A simple phase modulation of $\pm\pi/2$, which implies that the interferometer operates alternately at the right and left sides of the central fringe, is not sufficient, as in that case B_i is still null for null vibration noise. With a three-phase modulation $(-\pi/2, 0, \pi/2)$, $B_i = 1$ for null vibration noise, and replacing $\frac{B_i}{1+B_i^2}$ with $\frac{B_i}{\sigma_B^2+B^2+B_i^2}$, with B the mean of B_is, guarantees the full efficiency of the lock, whatever the amplitude of vibration noise.

The lock technique can be further modified to first determine and servo the vibration phase coefficients η_j. The phase of the interferometer is $e + S_i + \delta\phi_i$, where $\delta\phi_i$ is a controlled additional phase shift (alternately $-\pi/2, 0, \pi/2$), and the vibration phase S_i is (best approximated by) $\Sigma\eta_j\phi^S_{{\rm vib},j}$, where $j = x, y, z$ and $\phi^S_{{\rm vib},j}$ is the phase shift calculated from the seismometer data along axis j. At the ith measurement, S_i is calculated by $\sum_{j=1}^3 \eta_{j,i}\phi^S_{{\rm vib},j,i}$, where $\eta_{j,i} = \eta_j - \delta\eta_{j,i}$. P_i is thus given by

$$P_i = a - b\cos\left(\delta\phi_i + \sum_{j=1}^3 \eta_{j,i}\phi^S_{{\rm vib},j,i} + e + \sum_{j=1}^3 \delta\eta_{j,i}\phi^S_{{\rm vib},j,i}\right),$$

$$P_i = a - b\left(\cos S_i - \left(e + \sum_{j=1}^3 \delta\eta_{j,i}\phi^S_{{\rm vib},j,i}\right)\sin S_i\right),$$

where $S_i = \delta\phi_i + \sum_{j=1}^3 \eta_{j,i}\phi^S_{{\rm vib},j,i}$.

Generalizing the algebra above, one gets

$$b\left(B_i e + \sum_{j=1}^3 C_{j,i}\delta\eta_{j,i}\right) = A_i, \tag{8}$$

where

$$\begin{aligned} C_{j,i} &= (\cos S_{i+1} - \cos S_i)(\phi^S_{{\rm vib},j,i-1}\sin S_{i-1} - \phi^S_{{\rm vib},j,i}\sin S_i) \\ &\quad - (\cos S_{i-1} - \cos S_i)(\phi^S_{{\rm vib},j,i+1}\sin S_{i+1} \\ &\quad - \phi^S_{{\rm vib},j,i}\sin S_i). \end{aligned}$$

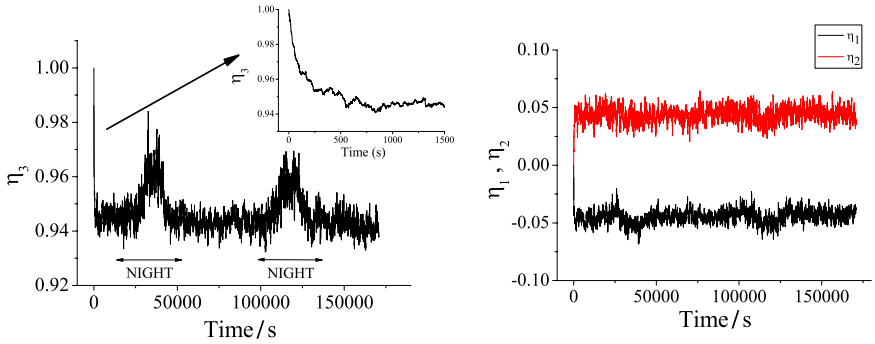

Figure 5. Evolution of the vibration phase coefficients, during a measurement realized using the non-linear lock scheme, with initial settings $\eta_{j,0} = (0, 0, 1)$. The graph on the left (respectively, right) displays the vertical (respectively, horizontal) phase coefficient(s).

Chirp rates and vibration phase coefficients are then corrected according to

$$\alpha_{i+2} = \alpha_{i+1} + K \frac{B_i}{\sigma_B^2 + B^2 + B_i^2} A_i,$$

$$\eta_{j,i+2} = \eta_{j,i+1} + L_j \frac{C_{j,i}}{\sigma_{C_j}^2 + C_{j,i}^2} A_i,$$

where L_j is the gain for direction j. Such non-linear feedback and estimation algorithms are inspired from Lyapounov stability theory, for the main loop given by equation (7), and adaptive techniques, for the estimation of parameters η_j (see [22] for a tutorial presentation of such techniques and [23] for a more advanced one).

Figure 5 displays the evolution of the vibration phase coefficients during a two-day measurement. The time constant of the lock is about 200 s (see inset). Note that the vertical phase coefficient η_3 differs significantly from 1 and is different at day and night times, which can be attributed to a change in the vibration noise PSD. Moreover, the lock converges towards horizontal phase coefficients of about 5%, in agreement with the values previously determined with the fit.

4.5. Comparison of the two techniques

Figure 6 displays the Allan standard deviation of g fluctuations for $2T = 100$ ms, with the two techniques described above (fringe fitting and non-linear lock), during day and night times. The vibration phase shifts were calculated from the 3D signals, using the optimal delay of 4.6 ms.

We obtain equivalent sensitivities at 1 s of $2.7 \times 10^{-7} g$ (respectively $1.8 \times 10^{-7} g$) with the non-linear lock (respectively fringe fitting) technique during the day and $8.5 \times 10^{-8} g$ (respectively $5.5 \times 10^{-8} g$) during the night. We find that the fit of the fringes is slightly better than the lock technique, by about 50%. The efficiency in removing vibration noise from the gravimeter signal can be calculated from the ratio of the sensitivities obtained here with the calculated contribution of the vibration noise (see section 2.3). A gain from 11 to 25 is obtained depending on the technique and noise conditions.

Best sensitivities are obtained during night measurements, as the vibration noise in the 1 Hz to 10 Hz band is significantly lower. We reach at best an equivalent sensitivity as low as

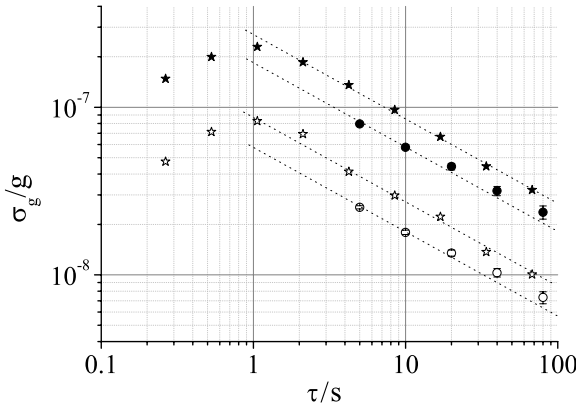

Figure 6. Allan standard deviation of g fluctuations versus averaging time. Measurements with the non-linear lock technique at day (respectively, at night) are displayed as full stars (respectively, open stars). Measurements with the fringe fitting technique at day (respectively, at night) are displayed as full circles (respectively, open circles).

$5.5 \times 10^{-8} g$ at 1 s when fitting fringes, which is only 4 times worse than our best reported value with the platform floating [12] and only twice as large as the sensitivity obtained in our laboratory with a commercial FG-5 corner cube gravimeter [2] in the same vibration noise conditions.

These two techniques were also compared in a numerical simulation, where the phase of the interferometer was generated randomly as the sum of two independent terms $\phi = \phi_1 + \phi_2$, with Gaussian distribution of standard deviations σ_1 and σ_2. ϕ_1 simulates the vibration phase noise measured by the seismometer ϕ_{vib}^S and ϕ_2 the phase difference between the real vibration phase noise and ϕ_{vib}^S. We then implemented the two techniques with such simulated data, with $\sigma_2 = 0.02$ rad and with σ_1 ranging from 0.06 rad to 30 rad. For each technique, we find the corresponding sensitivity of the interferometer at 1 shot σ_Φ and calculate a normalized sensitivity by dividing σ_Φ with σ_2. We verified that this normalized sensitivity does not depend on σ_2. The results of the simulations are displayed in figure 7 and for both techniques the normalized sensitivity exhibits the same behaviour. It increases for vibration noise larger than a few hundred millirads, for which linear approximation of the transition probability is no longer valid, and finally saturates for large vibration noise. This degradation is due to the non-linearity of the transition probability versus interferometer

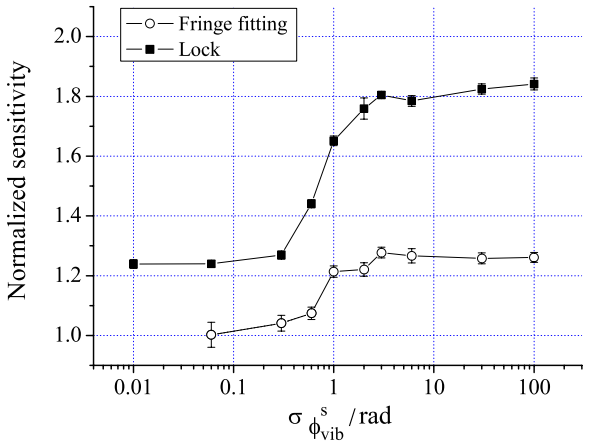

Figure 7. Numerical simulation of the normalized sensitivity of the interferometer as a function of the vibration noise standard deviation. Black squares (respectively, open circles) display the sensitivity degradation for the non-linear lock (respectively, fringe fitting) technique.

phase: measurements at top and bottom of the fringes have no sensitivity to phase fluctuations. The simulation confirms that this degradation is higher for the lock technique than for the fringe fitting technique, as observed in the measurements. In particular, for $\sigma_2 = 3$ rad, which corresponds roughly to day conditions, we find normalized sensitivities of 1.28 and 1.80 for the fringe fitting and lock techniques. The ratio of the sensitivities is thus 1.4, in reasonable agreement with the measurements.

4.6. Investigation of systematic effects

It is important to verify that the techniques presented here provide an accurate measurement of the interferometer phase, free from any bias. The lock procedure, which is intrinsically non-linear, could in principle induce such a bias. The numerical simulation indicates that neither of the two techniques suffers from such systematics. This was confirmed experimentally by performing differential measurements, alternating the standard integration technique described in section 2.2 with the lock procedure described in section 4.4, in the case where the platform was ON and thus the noise level low. The difference between the two techniques was found to be $0.3\,\mu\text{Gal} \pm 0.8\,\mu\text{Gal}$, which is consistent with no bias. Moreover, the two techniques were compared together during the day with the platform OFF, which corresponds to a noise level of $\sigma_{\phi^S_{\text{vib}}} = 3$ rad. The difference for a 6 h measurement was found to be $-2\,\text{mrad} \pm 4\,\text{mrad}$, which corresponds to $-5\,\mu\text{Gal} \pm 10\,\mu\text{Gal}$, which is also consistent with no bias.

4.7. Interest of the non-linear lock procedure

The main advantage of the non-linear lock scheme is a better time resolution. Indeed, the time constant of the lock loop can be reduced to a few cycles only, so that a time constant $\leqslant 1$ s can be reached. In comparison, fitting the fringes requires to fit data in packets of at least 20 cycles for optimal sensitivity, which reduces the time resolution to about 5 s. Both techniques can operate with low vibration noise. Indeed, the fit of the fringes can also be adapted by modifying the phase modulation to add measurements performed at the top and bottom of the interferometer, in order to constrain the sinusoidal fit (in doing so sensitivity will as well be degraded because these measurements are not sensitive to phase fluctuations). We finally illustrate the efficiency of the lock algorithm by demonstrating its robustness versus large changes in the vibration noise. Figure 8 displays the measurement during an earthquake of magnitude 7.7 that occurred in China on 20 March 2008. The gravimeter efficiently detects the occurrence of seismic waves, of period about 20 s. As our seismometer, of long period 30 s only, measures these vibrations with a large phase lag of about 1 rad, they are not efficiently removed from the gravimeter phase shift by the lock algorithm. They thus appear as a clear and well-resolved signal in the gravimeter data. This demonstrates the robustness of our system versus large excitations, which is not the case for traditional absolute corner cube gravimeters, which have neither adequate repetition rate (usually about 0.1 Hz) nor sufficient dynamic range, due to the finite range of the superspring mechanism. Note that the use of a longer period seismometer would in principle allow removal of these low frequency vibrations from the gravimeter data.

5. Conclusion

In this paper, we demonstrate that an atom interferometer can reach high sensitivities without vibration isolation, when using an independent measurement of vibrations by a low noise seismometer. We develop here several measurement protocols that allow determination of the mean phase of the interferometer, even when the interferometer phase noise amplitude exceeds 2π. In particular, fitting the fringes scanned by vibration noise allows one to reach a sensitivity as low as $5.5 \times 10^{-8} g$ at 1 s during night measurements. This performance is obtained with a rather short interaction time ($2T = 100$ ms), for which the vertical length of the interferometer corresponds to a few centimetres only.

The techniques presented here are of interest for the realization of a portable atom gravimeter, with potential application to geophysics and gravity measurements in noisy environments. A compact gravimeter associated with a good ac accelerometer and operating at a high repetition rate would reach fairly high sensitivities, without much hardware isolation against ground vibrations. Moreover, in contrast to other classical instruments, such as ballistic corner cube gravimeters, a high sensitivity would still be reached in the presence of earthquakes, if using a long period seismometer (100 s) to measure vibration noise. The technique demonstrated here could, for instance, be of interest for applications of atom interferometers to mobile gravimetry, in strap-down configuration.

More generally, these techniques can be extended to differential measurements with atom interferometers, such as gradiometers and cold atom gyroscopes. In particular, the phase difference can easily be extracted from the fits of the

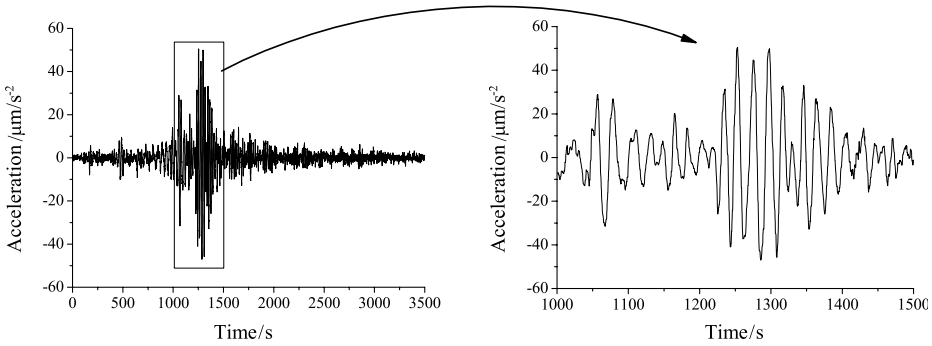

Figure 8. Fluctuations of the gravimeter signal during the earthquake of magnitude 7.7 that occurred in China on March 20, 2008. Data were obtained with the non-linear lock procedure.

two interference patterns. Much interest in these techniques lies in the ability to extend the dynamic range of the sensors and to extract the inertial phase without bias.

Acknowledgments

We would like to thank the Institut Francilien pour la Recherche sur les Atomes Froids (IFRAF) and the European Union (FINAQS) for financial support. QB and JLG, respectively, thank CNES and DGA for supporting their work.

References

[1] Bordé Ch J 1989 Atomic interferometry with internal state labeling *Phys. Lett.* A **140** 10
[2] Niebauer T M, Sasagawa G S, Faller J E, Hilt R and Klopping F 1995 A new generation of absolute gravimeters *Metrologia* **32** 159–80
[3] Fixler J B, Foster G T, McGuirk J M and Kasevich M A 2007 Atom interferometer measurement of the Newtonian constant of gravity *Science* **315** 74–7
[4] Lamporesi G, Bertoldi A, Cacciapuoti L, Prevedelli M and Tino G M 2008 Determination of the Newtonian gravitational constant using atom interferometry *Phys. Rev. Lett.* **100** 050801
[5] Wicht A, Hensley J M, Sarajlic E and Chu S 2002 A preliminary measurement of the fine structure constant based on atom interferometry *Phys. Scr.* **T102** 82–8
[6] Cladé P, de Mirandes E, Cadoret M, Guellati-Khélifa S, Schwob C, Nez F, Julien L and Biraben F 2006 Determination of the fine structure constant based on bloch oscillations of ultracold atoms in a vertical optical lattice *Phys. Rev. Lett.* **96** 033001
[7] Jacquey M, Büchner M, Trénec G and Vigué J 2007 First measurements of the index of refraction of gases for lithium atomic waves *Phys. Rev. Lett.* **98** 240405
[8] Kasevich M and Chu S 1991 Atomic interferometry using stimulated Raman transitions *Phys. Rev. Lett.* **67** 181–4
[9] Canuel B, Leduc F, Holleville D, Gauguet A, Fils J, Virdis A, Clairon A, Dimarcq N, Bordé Ch J, Landragin A and Bouyer P 2006 Six-axis inertial sensor using cold-atom interferometry *Phys. Rev. Lett.* **97** 010402
[10] Peters A, Chung K Y and Chu S 2001 High-precision gravity measurements using atom interferometry *Metrologia* **38** 25–61
[11] Hensley J M, Peters A and Chu S 1999 Active low frequency vertical vibration isolation *J. Sci. Instrum.* **70** 2735–41
[12] Le Gouët J, Mehlstäubler T E, Kim J, Merlet S, Clairon A, Landragin A, Pereira Dos Santos F 2008 Limits to the sensitivity of a low noise compact atomic gravimeter *Appl. Phys.* B **92** 133–44
[13] Müller H, Chiow S, Herrmann S, Chu S and Chung K Y 2008 Atom-interferometry tests of the isotropy of post-Newtonian gravity *Phys. Rev. Lett.* **100** 180405
[14] Canuteson E, Zumberge M and Hanson J 1997 An absolute method of vertical seismometer calibration by reference to a falling mass with application to the measurement of the gain *Bull. Seismol. Soc. Am.* **87** 484–93
[15] Brown J M, Niebauer T M and Klingele E 2001 Towards a dynamic absolute gravity system *Gravity, Geoid, and Geodynamics 2000, Int. Assoc. Geodesy (Banff, Canada, 31 July–4 August 2000)* vol 123 pp 223–8
[16] Genevès G *et al* 2005 The BNM Watt balance project *IEEE Trans. Instrum Meas.* **54** 850–3
[17] Merlet S, Kopaev A, Diament M, Genevès G, Landragin A and Pereira Dos Santos F 2008 Micro-gravity investigations for the LNE watt balance project *Metrologia* **45** 265–74
[18] Cheinet P, Pereira Dos Santos F, Petelski T, Le Gouët J, Kim J, Therkildsen K T, Clairon A and Landragin A 2006 Compact laser system for atom interferometry *Appl. Phys.* B **84** 643–6
[19] Bordé Ch J 2001 Theoretical tools for atom optics and interferometry *C.R. Acad. Sci. Paris, Série IV* **2** 509–30
[20] Baillard X, Gauguet A, Bize S, Lemonde P, Laurent Ph, Clairon A and Rosenbusch P 2006 Interference-filter-stabilized external-cavity diode lasers *Opt. Commun.* **266** 609–13
[21] Cheinet P, Canuel B, Pereira Dos Santos F, Gauguet A, Leduc F and Landragin A 2008 Measurement of the sensitivity function in a time-domain atomic interferometer *IEEE Trans. Instrum. Meas.* **57** 1141–8
[22] Slotine J J E and Li J W 1991 *Applied Nonlinear Control* (Englewood Cliffs, NJ: Prentice Hall)
[23] Khalil H K 1992 *Nonlinear Systems* (London: MacMillan)